
ADOPT: ADDITIVE OPTIMAL TRANSPORT REGRESSION

Wookyeong Song
 Department of Statistics
 University of California, Davis
 Davis, CA 95616, USA
 wksong@ucdavis.edu

Hans-Georg Müller
 Department of Statistics
 University of California, Davis
 Davis, CA 95616, USA
 hgmueeller@ucdavis.edu

ABSTRACT

Regression analysis for responses taking values in general metric spaces has received increasing attention, particularly for settings with Euclidean predictors $X \in \mathbb{R}^p$ and non-Euclidean responses $Y \in (\mathcal{M}, d)$. While additive regression is a powerful tool for enhancing interpretability and mitigating the curse of dimensionality in the presence of multivariate predictors, its direct extension is hindered by the absence of vector space operations in general metric spaces. We propose a novel framework for additive optimal transport regression, which incorporates additive structure through optimal geodesic transports. A key idea is to extend the notion of optimal transports in Wasserstein spaces to general geodesic metric spaces. This unified approach accommodates a wide range of responses, including probability distributions, symmetric positive definite (SPD) matrices with various metrics and spherical data. The practical utility of the method is illustrated with correlation matrices derived from resting state fMRI brain imaging data.

Keywords Additive Model · Optimal Transport · Metric Statistics

1 Introduction

We study regression where the response is a random object Y in a geodesic space (\mathcal{M}, d) with general metric d and the predictor is Euclidean $X \in \mathbb{R}^p$. Such settings arise widely for modern non-Euclidean data [33, 34], including diffusion tensor imaging in the space of symmetric positive definite matrices [27], mortality analysis in the space of one-dimensional probability distributions with the Wasserstein geometry [7], functional brain networks data [14, 44], corpus linguistics data on Riemannian manifolds [35], functional data [39] and many others [13, 29].

Local Fréchet regression extends kernel-based local linear regression to metric-valued responses [33, 8, 34]. However, like standard nonparametric regression, it suffers from the curse of dimensionality when $p > 1$, which limits its practical use for multivariate predictors. Dimension reduction via single-index models has been proposed to address this issue [3, 4, 17, 22, 43], but compressing predictor information into a single index may be too restrictive in some cases and then lead to biases. For the case of Euclidean responses, additive models have been shown to provide a competitive alternative that mitigates the curse of dimensionality while offering interpretability and flexibility [28, 41].

The generalization of additive models for metric space-valued responses is challenging because vector space operations, such as addition or scalar multiplication are unavailable in general metric spaces. Existing work covers additive structures for non-Euclidean responses only in some specialized settings, such as Hilbert space-valued responses [23], distributional responses via extrinsic approaches [20] and Lie group-valued data [27]. We introduce a novel additive framework based on geodesic optimal transports that generalize optimal transports in Wasserstein spaces to scenarios that feature general geodesic metric spaces. To estimate the additive transport map, we develop a transport backfitting algorithm, which is an extension of the popular classical backfitting method [5, 21].

Outline of the paper: In Section 2 and 3 we review related works and preliminaries regarding Fréchet means, local Fréchet regression and geodesic optimal transport. Section 4 presents the proposed additive optimal transport regression

(ADOPT) model and associated estimation procedure using a transport backfitting algorithm and theory on oracle convergence. Section 5 reports numerical experiments and Section 6 real data illustrations for fMRI correlation matrices.

2 Related Work

Prevalence of non-Euclidean data in recent years has created demand for principled and interpretable statistical tools for their analysis. A promising approach is to treat the sample elements as points in a metric space (\mathcal{M}, d) [11, 40]. Unlike Euclidean settings, general metric spaces lack algebraic structure, motivating distance-based statistical methods. The selected metric can greatly affect statistically relevant properties of the metric space [37]. For example for the case of symmetric positive definite (SPD) matrices the log-Cholesky metric [26] has desirable properties such as avoiding the swelling effect and allowing for closed-form parallel transport along geodesics.

The regression analysis of metric-valued responses has been studied in specialized scenarios [42, 10]. A general approach is Fréchet regression [33], based on the concept of conditional Fréchet means. Fréchet regression makes use of the vector space structure of predictors in \mathbb{R}^p to find elements in the metric space that minimize a weighted squared distances, and various extensions have been developed [36].

For distributional responses with the Wasserstein metric, geodesics are represented by optimal transport maps, enabling rich statistical applications [9]. Transport-based regression models have been developed for distribution-on-distribution regression [16] and autoregressive models [45]. [46] proposed a multiple regression framework via transport maps. However nonparametric additive extensions based on the intrinsic geometry of the space rather than extrinsic transformations have remained unexplored. We address this here by proposing a novel intrinsic metric framework for additive regression.

3 Preliminaries

3.1 Fréchet mean and Fréchet regression

Let (\mathcal{M}, d) be a metric space with distance $d : \mathcal{M} \times \mathcal{M} \rightarrow \mathbb{R}$. Consider random objects $(\mathbf{X}, Y) \sim \mathcal{F}$, where \mathcal{F} is their joint distribution, $\mathbf{X} = (X_1, \dots, X_p) \in \prod_{j=1}^p \mathcal{X}_j$ with compact domain $\mathcal{X}_j \subset \mathbb{R}$, and $Y \in \mathcal{M}$.

The Fréchet mean [15] generalizes the Euclidean expectation to random objects Y situated in metric spaces, with population and sample versions

$$\mathbb{E}_{\oplus} Y = \arg \min_{v \in \mathcal{M}} \mathbb{E} d^2(Y, v), \quad (1)$$

$$\hat{\mathbb{E}}_{\oplus} Y = \arg \min_{v \in \mathcal{M}} \frac{1}{n} \sum_{i=1}^n d^2(Y_i, v). \quad (2)$$

Since \mathcal{M} lacks vector space structure, Euclidean regression models cannot be directly applied. The Fréchet regression function is an implementation of conditional Fréchet means, extending conditional expectation to metric-valued responses:

$$\mathbb{E}_{\oplus}[Y \mid \mathbf{X} = \mathbf{x}] = \arg \min_{v \in \mathcal{M}} \mathbb{E}\{d^2(Y, v) \mid \mathbf{X} = \mathbf{x}\}.$$

For scalar responses $Y \in \mathbb{R}$, Fréchet conditional means reduce to the standard conditional expectation.

Local Fréchet regression [33] adapts local linear regression by replacing Euclidean distances with d and using kernel-based weights. We consider the univariate predictor $X \in \mathbb{R}$ with kernel K , bandwidth $h > 0$, and rescaled kernel $K_h(\cdot) = h^{-1}K(\cdot/h)$, where the extension to $X \in \mathbb{R}^p$ with $p > 1$ is straightforward. This leads to

$$\mathbb{E}_{\oplus L}[Y \mid X = x] = \arg \min_{v \in \mathcal{M}} \mathbb{E}\{w(x, h)d^2(Y, v)\},$$

with $w(x, h) = K_h(X - x)\{u_2 - u_1(X - x)\}/\sigma_0^2$, $u_j = \mathbb{E}\{K_h(X - x)(X - x)^j\}$, $j = 0, 1, 2$ and $\sigma_0^2 = u_0u_2 - u_1^2$.

Given random samples $(X_i, Y_i) \in \mathbb{R} \times \mathcal{M}$, $i = 1, 2, \dots, n$, the corresponding sample estimator is

$$\hat{\mathbb{E}}_{\oplus L}[Y \mid X = x] = \arg \min_{v \in \mathcal{M}} \frac{1}{n} \sum_{i=1}^n \hat{w}_i(x, h)d^2(Y_i, v), \quad (3)$$

where $\hat{w}_i(x, h) = K_h(X_i - x)\{\hat{u}_2 - \hat{u}_1(X_i - x)\}/\hat{\sigma}_0^2$,

with $\hat{u}_j = n^{-1} \sum_{i=1}^n K_h(X_i - x)(X_i - x)^j$ for $j = 0, 1, 2$ and $\hat{\sigma}_0^2 = \hat{u}_0 \hat{u}_2 - \hat{u}_1^2$. For various asymptotic results on the convergence of this estimator see [33, 8].

3.2 Geodesic optimal transport

For a metric space (\mathcal{M}, d) , the length of a path $\gamma : [0, 1] \rightarrow \mathcal{M}$ is defined as

$$l(\gamma) = \sup_{0=t_0 < t_1 < \dots < t_n=1, n \in \mathbb{N}} \sum_{i=1}^n d(\gamma(t_{i-1}), \gamma(t_i)).$$

A path γ_{v_1, v_2} is a geodesic from v_1 to v_2 if $\gamma_{v_1, v_2}(0) = v_1$, $\gamma_{v_1, v_2}(1) = v_2$ and $d(\gamma_{v_1, v_2}(t), \gamma_{v_1, v_2}(t')) \propto |t - t'|$ for all $t, t' \in [0, 1]$. A metric space (\mathcal{M}, d) is called a geodesic space if every pair of points $v_1, v_2 \in \mathcal{M}$ can be joined by a geodesic, and a unique geodesic space if this geodesic is unique [6, 25]. In Euclidean space, geodesics are straight lines that connect two points. Throughout we assume that (\mathcal{M}, d) is a bounded, separable, and uniquely geodesic space. For geodesic optimal transports, we require the following assumption [46]:

Assumption 1 For any random objects $v_1, v_2, v_3 \in \mathcal{M}$, where $v_1 \neq v_2$, there exists a map $\Gamma : \mathcal{M} \times \mathcal{M} \times \mathcal{M} \rightarrow \mathcal{M}$ and a unique element $v_4 \in \mathcal{M}$ such that

$$\Gamma(v_1, \gamma_{v_1, v_2}(r), v_3) = \gamma_{v_3, v_4}(r),$$

for any $r \in [0, 1]$.

In Euclidean space \mathbb{R}^p , the map is given by $\Gamma(v_1, \gamma_{v_1, v_2}(r), v_3) = v_3 + r(v_2 - v_1)$, for $r \in [0, 1]$, and $v_4 = v_3 + (v_2 - v_1)$.

Definition 1 (Geodesic optimal transport) Under Assumption 1, for any random objects $v_1, v_2 \in \mathcal{M}$, the geodesic transport and inverse geodesic transport from v_1 to v_2 , denoted as $T_{v_1, v_2} : \mathcal{M} \rightarrow \mathcal{M}$, $T_{v_1, v_2}^{-1} : \mathcal{M} \rightarrow \mathcal{M}$, respectively, are defined as

$$T_{v_1, v_2}(v) = \Gamma(v_1, v_2, v), \quad T_{v_1, v_2}^{-1}(v) = \Gamma(v_2, v_1, v),$$

for all $v \in \mathcal{M}$. Furthermore, the set of all geodesic transports maps is $\mathcal{T} = \{T_{v_1, v_2} : v_1, v_2 \in \mathcal{M}\}$.

We introduce an addition operation in the transport space \mathcal{T} as function composition:

$$T_{v_1, v_2} \oplus T_{v_3, v_4} = T_{v_3, v_4} \circ T_{v_1, v_2},$$

for any $T_{v_1, v_2}, T_{v_3, v_4} \in \mathcal{T}$ [45].

Example 1 (Space of distributional data with the Wasserstein metric)

Let $(\mathcal{W}_2(\mathcal{D}), d)$ be the space of one-dimensional probability distributions on a compact domain $\mathcal{D} \subset \mathbb{R}$ with finite second moments with 2-Wasserstein metric d ,

$$d^2(v_1, v_2) = \int_0^1 \{F_1^{-1}(s) - F_2^{-1}(s)\}^2 ds,$$

where $F_1^{-1}(\cdot)$ and $F_2^{-1}(\cdot)$ are the quantile functions of v_1 and v_2 , respectively.

Let $v \in \mathcal{W}_2(\mathcal{D})$ be a random element of $(\mathcal{W}_2(\mathcal{D}), d)$. For any measurable function $l : \mathcal{D} \rightarrow \mathcal{D}$ and $v \in \mathcal{W}_2(\mathcal{D})$, let $l\#v$ denote the push-forward measure of v , satisfying $l\#v(A) = v(\{x : l(x) \in A\})$ for all $A \in \mathcal{B}(\mathcal{D})$, the Borel σ -algebra on \mathcal{D} . For any two distributions $v_1, v_2 \in \mathcal{W}_2(\mathcal{D})$, the optimal transport map is

$$OT_{v_1, v_2} = F_2^{-1} \circ F_1.$$

The geodesic γ_{v_1, v_2} is given by McCann's interpolant [30],

$$\gamma_{v_1, v_2}(r) = (\text{id} + r(OT_{v_1, v_2} - \text{id}))\#v_1, \quad r \in [0, 1],$$

where $\text{id} : \mathcal{D} \rightarrow \mathcal{D}$ is the identity map. For notational convenience, we simply write $\mathcal{W}_2(\mathcal{D})$ as \mathcal{W}_2 .

For any random objects, $v_1, v_2, v_3 \in \mathcal{W}_2$, where $v_1 \neq v_2$, assumption 1 is satisfied with

$$\begin{aligned} \Gamma(v_1, \gamma_{v_1, v_2}(r), v_3) &= (\text{id} + r(OT_{v_1, v_2} - \text{id}))\#v_3 \\ &= \gamma_{v_3, v_4}(r), \quad r \in [0, 1], \end{aligned}$$

where $v_4 = T_{v_1, v_2}(v_3) = OT_{v_1, v_2} \# v_3$.

Example 2 (SPD matrices with the log-Cholesky metric)

Let \mathcal{S}_m^+ be the collection of $m \times m$ SPD matrices. For any $S \in \mathcal{S}_m^+$, there exists a unique lower triangular matrix L from the Cholesky decomposition, such that $S = LL^T$, where L is composed of $[L]$, the strictly lower triangular part, and $D(L)$, the diagonal part. The log-Cholesky metric is defined as

$$d^2(S_1, S_2) = \|[L_1] - [L_2]\|^2 + \|D(L_1) - D(L_2)\|^2,$$

where $S_1 = L_1L_1^T$, $S_2 = L_2L_2^T$, and $\|\cdot\|$ is the Frobenius norm. The geodesic γ_{S_1, S_2} is given by

$$\begin{aligned} \gamma_{S_1, S_2}(r) &= L(r)L(r)^T, \\ L(r) &= [L_1] + r([L_2] - [L_1]) \\ &\quad + \exp[\log(D(L_1)) + r(\log(D(L_2)) - \log(D(L_1)))], \end{aligned}$$

for any $r \in [0, 1]$. For any random objects, $S_1, S_2, S_3 \in \mathcal{S}_m^+$, where $S_1 \neq S_2$ and $S_3 = L_3L_3^T$, Assumption 1 is satisfied for all $r \in [0, 1]$ with

$$\begin{aligned} \Gamma(S_1, \gamma_{S_1, S_2}(r), S_3) &= L_\Gamma(r)L_\Gamma(r)^T = \gamma_{S_3, S_4}(r), \\ L_\Gamma(r) &= [L_3] + r([L_2] - [L_1]) \\ &\quad + \exp[\log(D(L_3)) + r(\log(D(L_2)) - \log(D(L_1)))], \end{aligned}$$

$$S_3 = L_3L_3^T, S_4 = L_\Gamma(1)L_\Gamma(1)^T.$$

Geodesic transports satisfying Assumption 1 can be constructed for several metrics on \mathcal{S}_m^+ including the Frobenius and power Frobenius metric and also for the space of graph Laplacians representing networks [46].

4 Additive Optimal Transport Regression

4.1 Population Model

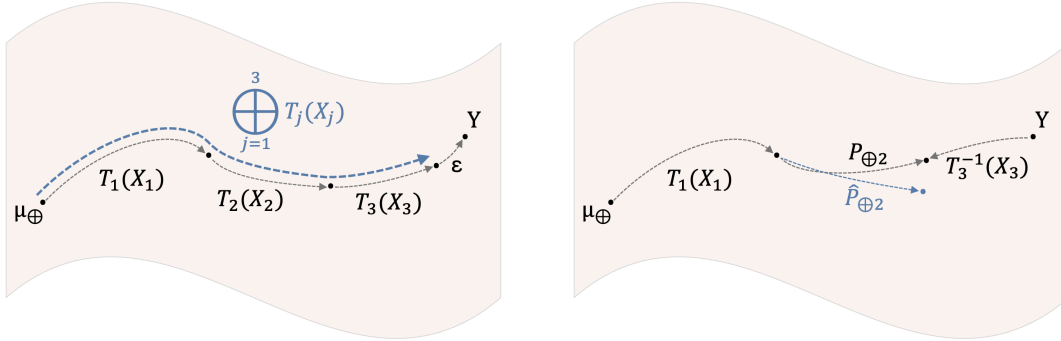


Figure 1: (Left panel) Additive optimal transport regression (ADOPT) framework with 3-dimensional predictors $X \in \mathbb{R}^3$ in (7). (Right panel) Population partial transport residual $P_{\oplus j}$ in (8) and its estimator $\hat{P}_{\oplus j}$ in (10) with $j = 2$.

We propose an additive optimal transport regression model that allows to regress Y on the high dimensional predictors \mathbf{X} . We first consider a scalar response $Y \in \mathbb{R}$ with predictors $\mathbf{X} = (X_1, \dots, X_p)$. The classical additive regression model is the conditional mean of response Y given $\mathbf{X} = \mathbf{x}$, defined as

$$m(\mathbf{x}) = \mathbb{E}[Y | \mathbf{X} = \mathbf{x}] = \beta_0 + g_1(x_1) + \dots + g_p(x_p), \quad (4)$$

with the assumptions that $\mathbb{E}Y = \beta_0$, and $\mathbb{E}g_j(X_j) = 0$, $j = 1, \dots, p$, for identifiability. Then, the classical additive regression model (4) is equivalent to

$$\begin{aligned} m(\mathbf{x}) &= (g_1(x_1) - \mathbb{E}g_1(X_1)) + \dots \\ &\quad + (g_p(x_p) - \mathbb{E}g_p(X_p)) + \mathbb{E}Y. \end{aligned} \quad (5)$$

In the case of scalar response $Y \in \mathbb{R}$ in (4), the j th additive term $g_j(X_j)$ is defined through conditional expectation of Y given $X_j = x_j$ is as follows:

$$\begin{aligned} m_j(x_j) &= \mathbb{E}[Y | X_j = x_j] = \mathbb{E}[\mathbb{E}[Y | \mathbf{X}] | X_j = x_j] \\ &= \mathbb{E}Y + g_j(x_j) + \mathbb{E}\left[\sum_{k \neq j} g_k(X_k) \mid X_j = x_j\right]. \end{aligned}$$

Then, the additive term $g_j(X_j)$ are given by

$$g_j(x_j) = \mathbb{E}[P_j | X_j = x_j],$$

where for $j = 1, \dots, p$ the j th partial residual is

$$P_j = (Y - \mathbb{E}Y) - \sum_{k \neq j} (g_k(X_k) - \mathbb{E}g_k(X_k)). \quad (6)$$

A direct extension of model (5) may not be feasible for responses situated in general metric spaces \mathcal{M} , since basic vector space operations, such as addition, scalar multiplication and expectation may not exist. We generalize the expectation \mathbb{E} to the Fréchet mean \mathbb{E}_\oplus in (1). For convenience we reuse the notation for the j th additive term g_j ,

$$g_j(x_j) \in \mathcal{M}, \quad x_j \in \mathcal{X}_j, \quad j = 1, \dots, p.$$

The difference between the j th additive term and its Fréchet mean is replaced by the geodesic transport pushing $\mathbb{E}_\oplus g_j(X_j)$ to $g_j(x_j)$, denoted as $T_j(x_j) := T_{\mathbb{E}_\oplus g_j(X_j), g_j(x_j)} \in \mathcal{T}$. Analogously, we introduce the j th inverse geodesic transport $T_j^{-1}(x_j) := T_{\mathbb{E}_\oplus g_j(X_j), g_j(x_j)}^{-1} \in \mathcal{T}$.

We further note that the actual responses in standard models (4) are $Y = m(\mathbf{x}) + \varepsilon$, however in metric spaces additive errors ε are not feasible. Contamination of responses by errors instead can be obtained through a random perturbation map $\mathcal{M} \rightarrow \mathcal{M}$ defined as $v' = \varepsilon(v)$, such that $\mathbb{E}_\oplus(v') = v$ and $\sigma^2 = \mathbb{E}d^2(v, v') > 0$ [8]. Assuming that the perturbation map is independent of predictors \mathbf{X} , this leads to the proposed ADOPT model

$$Y = \varepsilon(m_\oplus(\mathbf{x})) = \left[\bigoplus_{j=1}^p T_j(x_j) \oplus \varepsilon \right] (\mu_\oplus), \quad (7)$$

where $\mu_\oplus = \mathbb{E}_\oplus Y$ and $\bigoplus_{j=1}^p T_j = T_1 \oplus T_2 \oplus \dots \oplus T_p$.

Generalizing partial residuals in the conditional expectation, the j th partial transport residual $P_{\oplus j} \in \mathcal{T}$, $j = 1, \dots, p$, in the ADOPT model (7) is defined as

$$\begin{aligned} P_{\oplus j} &= [T_{j-1}^{-1}(X_{j-1}) \oplus \dots \oplus T_1^{-1}(X_1)] \oplus T_{\mu_\oplus, Y} \\ &\quad \oplus [T_p^{-1}(X_p) \dots \oplus T_{j+1}^{-1}(X_{j+1})]. \end{aligned} \quad (8)$$

The left panel of Figure 1 shows the framework of the additive optimal transport regression and the right panel the partial transport residual $P_{\oplus 2}$ for a 3-dimensional predictor $\mathbf{X} \in \mathbb{R}^3$.

4.2 Estimation

Given i.i.d. pairs $(\mathbf{X}_i, Y_i) \in \prod_{j=1}^p \mathcal{X}_j \times \mathcal{M}$, where $\mathbf{X}_i = (X_{i,1}, \dots, X_{i,p})$, the sample ADOPT model is

$$Y_i = \left[\bigoplus_{j=1}^p T_j(X_{i,j}) \oplus \varepsilon_i \right] (\mu_\oplus), \quad i = 1, \dots, n, \quad (9)$$

where we substitute the sample Fréchet mean (2) for the Fréchet mean μ_\oplus . To fit model (9), we apply standard backfitting [5, 21], an iterative algorithm with steps $t = 1, 2, \dots$, alternating between 1) a backfitting step, where the partial residual P_j in (6) is smoothed with respect to X_j , i.e., $g_j(x_j) \leftarrow \mathbb{E}(P_j | X = x_j)$, and 2) mean centering for identifiability, i.e., $g_j(x_j) \leftarrow g_j(x_j) - \mathbb{E}g_j(x_j)$, for all $j = 1, \dots, p$, until convergence. This alternating procedure is

applied separately for each predictor, cycling through the predictor set. We initialize with the Fréchet mean estimate $\hat{\mu}_\oplus$ and the identity maps $\hat{T}_j^{(0)}(\cdot) = \text{id}(\cdot) \in \mathcal{T}$, for $j = 1, 2, \dots, p$.

At each iteration $t = 1, 2, \dots$, we construct partial transport residuals

$$\begin{aligned} \hat{P}_{\oplus j}^{(t)} &= \left[\left(\hat{T}_{j-1}^{(t)} \right)^{-1} (X_{j-1}) \oplus \dots \oplus \left(\hat{T}_1^{(t)} \right)^{-1} (X_1) \right] \oplus \\ T_{\hat{\mu}_\oplus, Y} &\oplus \left[\left(\hat{T}_p^{(t-1)} \right)^{-1} (X_p) \dots \oplus \left(\hat{T}_{j+1}^{(t-1)} \right)^{-1} (X_{j+1}) \right], \end{aligned} \quad (10)$$

with sample observations $\hat{P}_{\oplus i, j}^{(t)}$ obtained by replacing (X_1, X_2, \dots, X_p) with $(X_{i,1}, X_{i,2}, \dots, X_{i,p})$, $i = 1, 2, \dots, n$. The right panel of Figure 1 illustrates the estimated partial transport residuals.

The transport backfitting step utilizes local Fréchet regression where the responses are the partial transport residuals, given each univariate predictor $X_j = x_j$,

$$\begin{aligned} g_j^{(t)}(x_j) &= \hat{\mathbb{E}}_{\oplus L} \left[\hat{P}_{\oplus j}^{(t)}(\hat{\mu}_\oplus) \mid X_j = x_j \right] \\ &= \arg \min_{v \in \mathcal{M}} \frac{1}{n} \sum_{i=1}^n \hat{w}_i(x_j, h) d^2 \left(\hat{P}_{\oplus i, j}^{(t)}(\hat{\mu}_\oplus), v \right). \end{aligned}$$

The weights \hat{w}_i are defined in (3) and the bandwidth h is selected by using 5-fold cross validation.

The mean centering step is generalized to a transport centering step,

$$\hat{T}_j^{(t)}(\cdot) = T_{\hat{\mathbb{E}}_{\oplus} g_j^{(t)}(X_j), g_j^{(t)}(\cdot)} \in \mathcal{T},$$

with sample Fréchet mean

$$\hat{\mathbb{E}}_{\oplus} g_j^{(t)}(X_j) = \arg \min_{v \in \mathcal{M}} \frac{1}{n} \sum_{i=1}^n d^2(g_j^{(t)}(X_{i,j}), v). \quad (11)$$

At iteration t , we apply the alternating steps cycling through predictors $X_j = x_j$, $j = 1, \dots, p$ and subsequently update the fitted responses

$$\hat{Y}_i^{(t)} = \left[\bigoplus_{j=1}^p \hat{T}_j^{(t)}(X_{i,j}) \right] (\hat{\mu}_\oplus), \quad i = 1, 2, \dots, n,$$

iterating until convergence when

$$\frac{1}{n} \sum_{i=1}^n d^2(\hat{Y}_i^{(t)}, \hat{Y}_i^{(t-1)}) < \epsilon,$$

for prespecified tolerance $\epsilon > 0$. The workflow is summarized in Algorithm 1.

Denote by $\hat{T}_j(\cdot)$ the estimates from Algorithm 1 when the other transports $T_1(\cdot), \dots, T_{j-1}(\cdot), T_{j+1}(\cdot), \dots, T_p(\cdot)$ are assumed to be known. Then one can obtain the following oracle convergence under mild assumptions (see the Supplement Section A for the proof and detailed assumptions).

Theorem 1 *Under Assumption 1 and the assumptions in Supplement Section A, if the bandwidth $h \rightarrow 0$ and $nh \rightarrow \infty$ as $n \rightarrow \infty$, it holds that*

$$d \left(T_j(x_j)(\nu), \hat{T}_j(x_j)(\nu) \right) = o_P(1),$$

for any $x_j \in \mathcal{X}_j$, and $\nu \in \mathcal{M}$.

5 Simulations

5.1 Distribution-valued responses with Wasserstein metric

We consider univariate distributional responses Y situated in the 2-Wasserstein space \mathcal{W}_2 with Euclidean predictor vectors $\mathbf{X} \in [0, 1]^3$, introduced in Example 1. In a slight abuse of notation, we use Y to denote the quantile function

Algorithm 1 Transport Backfitting Algorithm

Require: $(X_i, Y_i) \in \mathbb{R}^p \times \mathcal{M}$, $i = 1, 2, \dots, n$, and convergence tolerance $\epsilon > 0$.

Ensure: $\hat{T}_j(\cdot) \in \mathcal{T}$, $j = 1, 2, \dots, p$.

1: Initialize $\hat{T}_j^{(0)}(\cdot) = \text{id}$, $j = 1, \dots, p$, and $\hat{Y}_i^{(0)} = \left[\bigoplus_{j=1}^p \hat{T}_j^{(0)}(X_{i,j}) \right](\hat{\mu}_\oplus)$, $i = 1, 2, \dots, n$, with sample Fréchet mean $\hat{\mu}_\oplus$.

2: **for** $t = 1, 2, \dots$ until convergence **do**

3: **for** $j = 1, \dots, p$ **do**

4: Transport backfitting via local Fréchet regression $\hat{\mathbb{E}}_{\oplus L}$ in (3),

$$g_j^{(t)}(x_j) = \hat{\mathbb{E}}_{\oplus L} \left[\hat{P}_{\oplus j}^{(t)}(\hat{\mu}_\oplus) \mid X_j = x_j \right],$$

with partial transport residual observations $\hat{P}_{\oplus j}^{(t)}$ in (10).

5: Transport Centering,

$$\hat{T}_j^{(t)}(\cdot) = T_{\hat{\mathbb{E}}_{\oplus} g_j^{(t)}(X_j), g_j^{(t)}(\cdot)} \in \mathcal{T},$$

with Fréchet mean $\hat{\mathbb{E}}_{\oplus} g_j^{(t)}(X_j)$ in (11).

6: **end for**

7: $\hat{Y}_i^{(t)} = \left[\bigoplus_{j=1}^p \hat{T}_j^{(t)}(X_{i,j}) \right](\hat{\mu}_\oplus)$, $i = 1, 2, \dots, n$.

8: Stopping rule: Stop if

$$\frac{1}{n} \sum_{i=1}^n d^2(\hat{Y}_i^{(t)}, \hat{Y}_i^{(t-1)}) < \epsilon.$$

9: **end for**

corresponding to a distribution. We generate distributional responses from the additive transport regression model in (9),

$$Y_i = \left[\bigoplus_{j=1}^3 T_j(X_{i,j}) \oplus \varepsilon_i \right](U),$$

where $U = \text{Unif}(0, 1)$, $T_j(x_j) = T_{\mathbb{E}_{\oplus} g_j(X_j), g_j(x_j)}$, $x_j \in [0, 1]$, $j = 1, 2, 3$, and $\varepsilon_i(f)(u) = f(u) + \frac{1}{2\pi} \xi_i \sin(2\pi f(u))$, for all quantile functions $f \in \mathcal{W}_2$, and $u \in [0, 1]$, $\xi_i \sim \text{Unif}(-1, 1)$. We consider the following two cases:

- Case I (Beta distributions): Here $g_1(x_1) = \text{Beta}(1 + 2x_1, 1)$, $g_2(x_2) = \text{Beta}(1, 2 + 3x_2)$, and $g_3(x_3) = \text{Beta}(\frac{1}{2} + \frac{1}{2}x_3, \frac{1}{2} + \frac{1}{2}x_3)$.
- Case II (Normal distributions): Here $g_1(x_1) = N(x_1, 1)$, $g_2(x_2) = N(x_2^2, 1)$, and $g_3(x_3) = N(e^{-x_3}, 1)$.

We generate 3-dimensional Euclidean predictors $\mathbf{X}_i = (X_{i,1}, X_{i,2}, X_{i,3}) = (\Phi(V_{i,1}), \Phi(V_{i,2}), \Phi(V_{i,3}))^T$, $i = 1, \dots, n$, where Φ is the standard normal CDF and $\mathbf{V}_i = (V_{i,1}, V_{i,2}, V_{i,3})^T \sim N_3(\mathbf{0}, \Sigma)$, $\Sigma = \begin{pmatrix} 1 & 0.5 & 0.3 \\ 0.5 & 1 & 0.5 \\ 0.3 & 0.5 & 1 \end{pmatrix}$. For

each case, we generate $n = 100$, and 300 pairs of $(\mathbf{X}_i, \mathbf{Y}_i)$, $i = 1, 2, \dots, n$. We compare the finite-sample performance of the proposed ADOPT model with global Fréchet regression (GF) [33], additive functional regression [20] (ADR) and simply taking the constant Fréchet mean (FM), in terms of the approximated mean integrated squared error (MISE),

$$\text{MISE} \approx B^{-1} \sum_{b=1}^B \int_{[0,1]^3} d^2(\hat{Y}_{\mathbf{x}}^{(b)}, Y_{\mathbf{x}}) d\mathbf{x}, \quad (12)$$

where d is 2-Wasserstein distance, $\hat{Y}_{\mathbf{x}}^{(b)}$ with $\mathbf{x} = (x_1, x_2, x_3)$ are estimates from the b^{th} Monte Carlo (MC) samples $\{(\mathbf{X}_i^{(b)}, \mathbf{Y}_i^{(b)}) : 1 \leq i \leq n\}$, and $Y_{\mathbf{x}}$ are the true distributional data without noise, $Y_{\mathbf{x}} = \left[\bigoplus_{j=1}^p T_j(x_j) \right](U)$. The results are in Table 1 and demonstrate that ADOPT has the smallest MISE among the comparison methods and as n increases the MISE of ADOPT decreases, while this is not the case for the competing methods.

Table 1: Mean integrated squared error (MISE) results ($\times 10^{-3}$) with standard errors in parentheses under distributional responses in the Wasserstein space for two cases with different sample sizes $n = 100$, and 300 . We compare four methods: additive optimal transport regression (ADOPT), global Fréchet regression [33] (GF), additive functional regression [20] (ADR), and Fréchet mean [15] (FM) without predictor effect.

Case	n	Method			
		ADOPT	GF	ADR	FM
I	100	0.317 (0.010)	0.591 (0.008)	0.761 (0.008)	11.019 (0.068)
	300	0.181 (0.004)	0.499 (0.003)	0.586 (0.004)	11.119 (0.040)
II	100	1.685 (0.057)	6.636 (0.057)	80.411 (0.702)	207.205 (1.681)
	300	1.121 (0.041)	6.701 (0.037)	81.951 (0.455)	211.297 (1.080)

5.2 SPD matrices-valued response with log-Cholesky metric

We consider $m \times m$ SPD matrix valued responses $Y \in \mathcal{S}_m^+$ equipped with the log-Cholesky metric [26] introduced in Example 2, and Euclidean predictors $\mathbf{X} \in [0, 1]^3$ and generate SPD responses from the additive transport regression model in (9),

$$Y_i = \left[\bigoplus_{j=1}^3 T_j(X_{i,j}) \oplus \varepsilon_i \right] (\mathbf{I}_m) \in \mathcal{S}_m^+,$$

where \mathbf{I}_m is $m \times m$ identity matrix, $T_j(x_j) = T_{\mathbb{E}_{\oplus} g_j(X_j), g_j(x_j)}$, $j = 1, \dots, 3$, and for $S = LL^T \in \mathcal{S}_m^+$ with Cholesky decomposition, the perturbation error map $\varepsilon_i(S) = \varepsilon_i(LL^T) = e_i(L)e_i(L)^T$, where $e_i(L)_{k,l} = L_{k,l} + \xi_{k,l}$, and $\xi_{k,l} \sim N(0, \sigma^2)$, $k > l$, $e_i(L)_{k,l} = L_{k,l}$, when $k = l$, and $e_i(L)_{k,l} = 0$ if $k < l$.

We generate the transport map $T_j(x_j)$ based on

$$g_j(x_j) = L_j(x_j)L_j(x_j)^T, \quad x_j \in [0, 1], \quad j = 1, 2, 3,$$

with random Cholesky factors $L_j(x_j)$ which are lower triangular matrices as follows:

- Case I (Linear in \mathbf{x}):

$$\begin{aligned} (L_1(x_1))_{k,l} &= \exp^{-|k-l|/2} (x_1 + 1) / 2, \\ (L_2(x_2))_{k,l} &= \exp^{-|k-l|/3} (x_2 + 1) / 4, \\ (L_3(x_3))_{k,l} &= \exp^{-|k-l|/4} (x_3 + 1) / 8. \end{aligned}$$

- Case II (Non-linear in \mathbf{x}):

$$\begin{aligned} (L_1(x_1))_{k,l} &= \exp^{-|k-l|/2} \sin((x_1 + 1)\pi/4), \\ (L_2(x_2))_{k,l} &= \exp^{-|k-l|/4} (x_2^2 + 1) / 2, \\ (L_3(x_3))_{k,l} &= \exp^{-|k-l|/4} \exp^{-x_3}, \end{aligned}$$

for $k \geq l$, and all other elements are 0 if $k < l$.

We then generate random covariates $\mathbf{X}_i = (X_{i,1}, X_{i,2}, X_{i,3})$, $i = 1, \dots, n$, following the same procedure as in the distribution-valued simulations of Section 5.1. The responses are generated under each scenario with perturbations ε_i having standard deviation $\sigma = 0.01$. We sample $n = 100$ and 300 i.i.d. pairs of $(\mathbf{X}_i, Y_i) \in \mathbb{R}^3 \times \mathcal{S}_m^+$, with matrix sizes $m = 10$ and $m = 20$ and compare the finite sample performance of the proposed ADOPT with the global Fréchet regression (GF) and the constant Fréchet mean (FM) in terms of mean integrated squared error (MISE), analogously defined as in (12). Table 2 displays the MISEs for $B = 200$ with standard error in parentheses. ADOPT has the lowest MISE and its MISE decreases as the sample size n increases, while this is not the case for the competing methods. As the size of SPD matrices increases, the MISE increases, but ADOPT always has substantially better performance.

Table 2: Mean integrated squared error (MISE) results ($\times 10^{-2}$) with standard errors in parentheses for $m \times m$ SPD matrices as responses in \mathcal{S}_m^+ with the log-Cholesky metric for two simulation cases with different sample sizes $n = 100$, and 300 and matrix dimensions $m = 10$, and 20, comparing three methods: additive optimal transport regression (ADOPT), global Fréchet regression (GF) and Fréchet mean (FM).

Case	m	n	Method			
			ADOPT	GF	FM	
I	10	100	2.769 (0.025)	9.495 (0.060)	135.344 (0.647)	
		300	1.655 (0.012)	9.714 (0.037)	136.122 (0.366)	
	20	100	5.712 (0.070)	14.110 (0.102)	192.688 (0.92)	
		300	3.788 (0.048)	14.254 (0.063)	193.796 (0.521)	
	II	10	100	4.146 (0.088)	18.507 (0.090)	96.562 (0.490)
			300	2.702 (0.036)	18.808 (0.052)	97.047 (0.303)
20		100	8.921 (0.167)	28.237 (0.14)	143.382 (0.706)	
		300	6.435 (0.100)	28.512 (0.078)	144.088 (0.437)	

6 Brain connectivity for fMRI data

We use resting state functional Magnetic Resonance Imaging (rs-fMRI) data obtained from the Alzheimer’s Disease Neuroimaging Initiative (ADNI) database (`adni.loni.usc.edu`). Brain signal analysis at the subject level relies on time series of Blood Oxygen Level Dependent (BOLD) signals, obtained for a set of regions of interest (ROIs). The coherence between pairwise ROIs is customarily quantified by Pearson correlation coefficients of the rs-fMRI time series, leading to a $l \times l$ correlation matrix for l ROIs [2, 32]. Further details about BOLD signals, the list of $l = 11$ ROIs used in the analysis [1] and the construction of the correlation matrices from rs-fMRI brain imaging are described in Supplement Section B.

We analyze the 11×11 correlation matrices equipped with the log-Cholesky metric as responses using the ADOPT model in (9), based on $n = 929$ ADNI participants classified into six diagnostic stages: 248 cognitively normal (CN), 110 subjective memory complaint (SMC), 316 early mild cognitive impairment (EMCI), 12 mild cognitive impairment (MCI), and 171 late mild cognitive impairment (LMCI), and 72 Alzheimer’s disease (AD). For AD studies, cerebrospinal fluid amyloid-beta ($A\beta$) and phosphorylated tau (p-Tau) concentration are widely used markers of AD pathology [19, 24].

We consider $p = 3$ predictors: X_1 is $A\beta$ concentration ranging from 203 to 1700, with lower amyloid-beta signaling a worse prognosis; X_2 is the diagnostic stage coded ordinally from 0 to 5 in the order CN, SMC, EMCI, MCI, LMCI, AD; X_3 is the p-Tau concentration ranging from 8.00 to 92.08, with higher p-Tau typically indicating worse prognosis.

To compare brain coherence patterns across distinct risk profiles, we construct three covariate settings representing low, intermediate, and high risk groups. The low risk group corresponds to the upper 10% of $A\beta$ values (1700), the lower 10% disease stage (CN = 0), and p-Tau values (12.8). The intermediate risk group is defined by median values of $A\beta$ (995.8), disease stage (EMCI = 2), and p-Tau (21.94). The high risk group corresponds to the lower 10% of $A\beta$ values (535), the upper 90% disease stage (LMCI = 4), and p-Tau values (42.01).

Figure 2 displays each transport map $T_j(x_j) = T_{\mathbb{E}_{\oplus g}(X_j), g(x_j)}$ as the difference of the Cholesky factors of the two correlation matrices, i.e., $L_{g(x_j)} - L_{\mathbb{E}_{\oplus g}(X_j)}$, where L_S is a lower triangular Cholesky factor of SPD matrices $S \in \mathcal{S}_l^+$, with ROIs labeling rows and columns of each Cholesky factor. The estimated transport maps $T_1(x_1)$ (first column), $T_2(x_2)$ (second column), $T_3(x_3)$ (third column), and their combined effect $[T_1(x_1) \oplus T_2(x_2) \oplus T_3(x_3)]$ (fourth column)

are obtained from ADOPT. The rows correspond to the low, intermediate, and high risk groups, with covariates $\mathbf{x} = (x_1, x_2, x_3)$ defined in the previous paragraph. For the low risk group (first row), the transport maps generally indicate increasing correlations between ROIs, with the largest increase of 0.10 observed between pIPL and MPFC. For the intermediate group (second row), the transport maps are close to zero, implying that the Fréchet mean $\hat{\mu}_{\oplus}$ is similar to the estimated response $[T_1 \oplus T_2 \oplus T_3](\hat{\mu}_{\oplus})$. In contrast, the high risk group (third row) shows decreasing correlations, with the strongest decline of 0.11 between pIPL and MPFC.

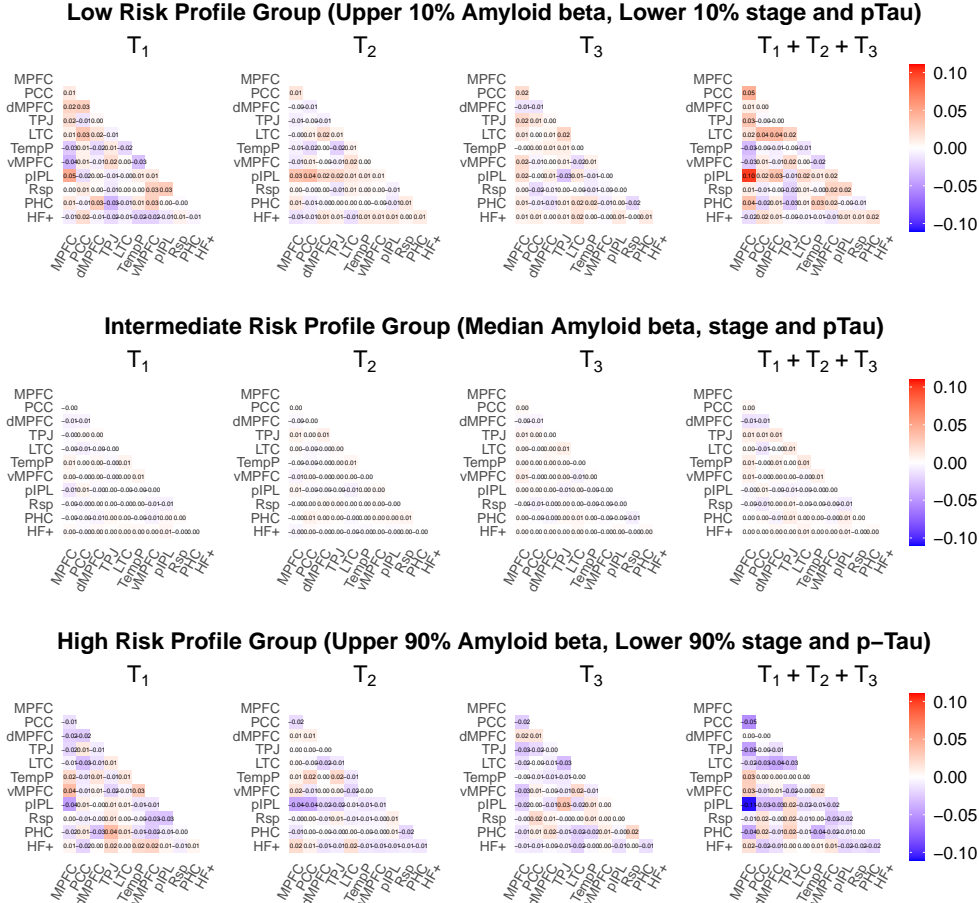


Figure 2: Estimated transport maps $T_1(x_1)$ (first column), $T_2(x_2)$ (second column), $T_3(x_3)$ (third column), and their combined map $[T_1(x_1) \oplus T_2(x_2) \oplus T_3(x_3)]$ (fourth column) represented as the difference of the lower triangular Cholesky factors, with regions of interest (ROIs) labeling rows and columns of each Cholesky factor. Rows correspond to low, intermediate, and high risk groups, with covariates $\mathbf{x} = (x_1, x_2, x_3)$ defined as follows: the low risk group corresponds to the upper 10% of $A\beta$ values (1700), the lower 10% disease stage (CN = 0), and p-Tau values (12.8); the intermediate group is defined by the median $A\beta$ value (995.8), median disease stage (EMCI = 2), and median p-Tau value (21.94); and the high risk group corresponds to the upper 90% of $A\beta$ values (535), the lower 90% disease stage (LMCI = 4), and p-Tau values (42.01).

We evaluate out-of-sample prediction performance using 5-fold cross-validation. Specifically, we partition the index set $1, \dots, n$ into disjoint folds \mathcal{I}_q ($q = 1, \dots, 5$) with $n_q = |\mathcal{I}_q|$. For each fold, we define the Mean Prediction Error Reduction (MPER) as

$$\text{MPER} = \frac{1}{5} \sum_{q=1}^5 \text{MPER}_q,$$

$$\text{MPER}_q = \frac{1}{n_q} \sum_{i \in \mathcal{I}_q} \left\{ d(\hat{\mu}_{\oplus}^{(-q)}, Y_i) - d(\hat{Y}_i^{(-q)}, Y_i) \right\},$$

where $\hat{Y}_i^{(-q)}$ is the predicted response from the regression model trained on the remaining folds, $\hat{\mu}_{\oplus}^{(-q)}$ is the Fréchet mean of the training responses (baseline without predictors), and d is the log-Cholesky metric. MPER measures the reduction in prediction error relative to the baseline; larger values indicate better predictive performance. We compare our method against global Fréchet regression (GF) [33]. The average of MPER ($\times 10^{-4}$) obtained for $B = 200$ Monte Carlo simulations is 2.625 (0.055) for ADOPT and 1.713 (0.052) for global Fréchet regression (with standard errors in parentheses). This demonstrates that ADOPT improves out-of-sample performance substantially in terms of MPER.

7 Discussion

We develop ADOPT, an additive optimal transport regression approach for random object responses with multivariate continuous Euclidean predictors, thereby providing a flexible regression model for metric space-valued responses that addresses the curse of dimensionality and enhancing interpretability in real data analysis. The method is built on an extension of optimal transport ideas to general metric spaces and utilizes a transport map for each predictor.

We illustrate the interpretability of ADOPT with brain connectivity for resting state fMRI brain imaging data. Numerical experiments with distributional responses in Wasserstein space and SPD matrices with the log-Cholesky metric also demonstrate strong performance of the proposed ADOPT.

References

- [1] Jessica R Andrews-Hanna, Jay S Reidler, Jorge Sepulcre, Renee Poulin, and Randy L Buckner. Functional-anatomic fractionation of the brain’s default network. *Neuron*, 65(4):550–562, 2010.
- [2] AmanPreet Badhwar, Angela Tam, Christian Dansereau, Pierre Orban, Felix Hoffstaedter, and Pierre Bellec. Resting-state network dysfunction in Alzheimer’s disease: a systematic review and meta-analysis. *Alzheimer’s & Dementia: Diagnosis, Assessment & Disease Monitoring*, 8:73–85, 2017.
- [3] Satarupa Bhattacharjee, Bing Li, and Lingzhou Xue. Nonlinear global Fréchet regression for random objects via weak conditional expectation. *The Annals of Statistics*, 53(1):117–143, 2025.
- [4] Satarupa Bhattacharjee and Hans-Georg Müller. Single index Fréchet regression. *The Annals of Statistics*, 51(4):1770–1798, 2023.
- [5] Leo Breiman and Jerome H Friedman. Estimating optimal transformations for multiple regression and correlation. *Journal of the American statistical Association*, 80(391):580–598, 1985.
- [6] Dmitri Burago, Yuri Burago, and Sergei Ivanov. *A Course in Metric Geometry*, volume 33. American Mathematical Society, 2022.
- [7] Yaqing Chen, Zhenhua Lin, and Hans-Georg Müller. Wasserstein regression. *Journal of the American Statistical Association*, 118(542):869–882, 2023.
- [8] Yaqing Chen and Hans-Georg Müller. Uniform convergence of local Fréchet regression with applications to locating extrema and time warping for metric space valued trajectories. *The Annals of Statistics*, 50(3):1573–1592, 2022.
- [9] Sinho Chewi, Jonathan Niles-Weed, and Philippe Rigollet. Statistical optimal transport. *arXiv preprint arXiv:2407.18163*, 3, 2024.
- [10] Emil Cornea, Hongtu Zhu, Peter Kim, and Joseph G. Ibrahim. Regression models on Riemannian symmetric spaces. *Journal of the Royal Statistical Society: Series B (Statistical Methodology)*, 79(2):463–482, 2017.
- [11] Paromita Dubey, Yaqing Chen, and Hans-Georg Müller. Metric statistics: Exploration and inference for random objects with distance profiles. *The Annals of Statistics*, 52(2):757–792, 2024.
- [12] Paromita Dubey and Hans-Georg Müller. Fréchet analysis of variance for random objects. *Biometrika*, 106(4):803–821, 2019.
- [13] P Thomas Fletcher. Geodesic regression and the theory of least squares on riemannian manifolds. *International journal of computer vision*, 105(2):171–185, 2013.
- [14] Alex Fornito, Andrew Zalesky, and Edward Bullmore. *Fundamentals of Brain Network Analysis*. Academic press, 2016.
- [15] Maurice Fréchet. Les éléments aléatoires de nature quelconque dans un espace distancié. *Annales de l’Institut Henri Poincaré*, 10(4):215–310, 1948.

- [16] Laya Ghodrati and Victor M Panaretos. Distribution-on-distribution regression via optimal transport maps. *Biometrika*, 109(4):957–974, 2022.
- [17] Aritra Ghosal, Wendy Meiring, and Alexander Petersen. Fréchet single index models for object response regression. *Electronic Journal of Statistics*, 17(1):1074–1112, 2023.
- [18] Peter Hall, Hans-Georg Müller, and Fang Yao. Modelling sparse generalized longitudinal observations with latent gaussian processes. *Journal of the Royal Statistical Society Series B: Statistical Methodology*, 70(4):703–723, 2008.
- [19] Harald Hampel, John Hardy, Kaj Blennow, Christopher Chen, George Perry, Seung Hyun Kim, Victor L Villenave, Paul Aisen, Michele Vendruscolo, Takeshi Iwatsubo, et al. The amyloid- β pathway in Alzheimer’s disease. *Molecular psychiatry*, 26(10):5481–5503, 2021.
- [20] Kyunghye Han, Hans-Georg Müller, and Byeong U Park. Additive functional regression for densities as responses. *Journal of the American Statistical Association*, 115(530):997–1010, 2020.
- [21] Trevor Hastie and Robert Tibshirani. Generalized additive models. *Statistical science*, 1(3):297–310, 1986.
- [22] Houren Hong, Janice L Scealy, Andrew TA Wood, and Yanrong Yang. A robust extrinsic single-index model for spherical data. *arXiv preprint arXiv:2503.24003*, 2025.
- [23] Jeong Min Jeon and Byeong U Park. Additive regression with Hilbertian responses. *The Annals of Statistics*, 48(5):2671–2697, 2020.
- [24] Thomas K Karikari, Nicholas J Ashton, Gunnar Brinkmalm, Wagner S Brum, Andréa L Benedet, Laia Montoliu-Gaya, Juan Lantero-Rodriguez, Tharick Ali Pascoal, Marc Suárez-Calvet, Pedro Rosa-Neto, et al. Blood phospho-tau in alzheimer disease: analysis, interpretation, and clinical utility. *Nature Reviews Neurology*, 18(7):400–418, 2022.
- [25] Serge Lang. *Differential and Riemannian manifolds*, volume 160. Springer Science & Business Media, 2012.
- [26] Zhenhua Lin. Riemannian geometry of symmetric positive definite matrices via cholesky decomposition. *SIAM Journal on Matrix Analysis and Applications*, 40(4):1353–1370, 2019.
- [27] Zhenhua Lin, Hans-Georg Müller, and Byeong U Park. Additive models for symmetric positive-definite matrices and Lie groups. *Biometrika*, 110(2):361–379, 2023.
- [28] Oliver Linton and Jens Perch Nielsen. A kernel method of estimating structured nonparametric regression based on marginal integration. *Biometrika*, pages 93–100, 1995.
- [29] James Stephen Marron and Ian L Dryden. *Object Oriented Data Analysis*. Chapman and Hall/CRC, 2021.
- [30] Robert J McCann. A convexity principle for interacting gases. *Advances in mathematics*, 128(1):153–179, 1997.
- [31] M Paul Murphy and Harry LeVine III. Alzheimer’s disease and the amyloid- β peptide. *Journal of Alzheimer’s disease*, 19(1):311–323, 2010.
- [32] Matej Perovnik, Tomaz Rus, Katharina A Schindlbeck, and David Eidelberg. Functional brain networks in the evaluation of patients with neurodegenerative disorders. *Nature Reviews Neurology*, 19(2):73–90, 2023.
- [33] Alexander Petersen and Hans-Georg Müller. Fréchet regression for random objects with Euclidean predictors. *The Annals of Statistics*, 47:691–719, 2019.
- [34] Christof Schötz. Nonparametric regression in nonstandard spaces. *Electronic Journal of Statistics*, 16(2):4679–4741, 2022.
- [35] Katie E Severn, Ian L Dryden, and Simon P Preston. Manifold valued data analysis of samples of networks, with applications in corpus linguistics. *The Annals of Applied Statistics*, 16(1):368–390, 2022.
- [36] Dogyoon Song and Kyunghye Han. Errors-in-variables Fréchet regression with low-rank covariate approximation. *Advances in Neural Information Processing Systems*, 36:80575–80607, 2023.
- [37] Wookyeong Song and Hans-Georg Müller. Inference for dispersion and curvature of random objects. *Journal of the American Statistical Association*, pages 1–23, 2025.
- [38] AW van der Vaart and Jon A Wellner. *Weak Convergence and Empirical Processes: With Applications to Statistics*. Springer Nature, 2023.
- [39] Jane-Ling Wang, Jeng-Min Chiou, and Hans-Georg Müller. Functional data analysis. *Annual Review of Statistics and its application*, 3:257–295, 2016.
- [40] Xueqin Wang, Jin Zhu, Wenliang Pan, Junhao Zhu, and Heping Zhang. Nonparametric statistical inference via metric distribution function in metric spaces. *Journal of the American Statistical Association*, 119(548):2772–2784, 2024.

- [41] Kyusang Yu, Byeong U Park, and Enno Mammen. Smooth backfitting in generalized additive models. *The Annals of Statistics*, 36(1):228–260, 2008.
- [42] Ying Yuan, Hongtu Zhu, Weili Lin, and JS Marron. Local polynomial regression for symmetric positive definite matrices. *Journal of the Royal Statistical Society: Series B (Statistical Methodology)*, 74(4):697–719, 2012.
- [43] Qi Zhang, Lingzhou Xue, and Bing Li. Dimension reduction for Fréchet regression. *Journal of the American Statistical Association*, 119(548):2733–2747, 2024.
- [44] Yidong Zhou and Hans-Georg Müller. Network regression with graph Laplacians. *Journal of Machine Learning Research*, 23(320):1–41, 2022.
- [45] Changbo Zhu and Hans-Georg Müller. Autoregressive optimal transport models. *Journal of the Royal Statistical Society Series B: Statistical Methodology*, 85(3):1012–1033, 2023.
- [46] Changbo Zhu and Hans-Georg Müller. Geodesic optimal transport regression. *Biometrika*, page asaf086, 2025.

A Technical Details

A.1 Assumptions

In this section, we state the assumptions required for Theorem 1 and introduce the necessary notation. For all $\nu \in \mathcal{M}$ and $T_j \in \mathcal{T}$, $j = 1, \dots, p$, define $Z_j(x_j) = [\varepsilon \circ T_j(x_j)](\nu) \in \mathcal{M}$, $x_j \in \mathcal{X}_j$, where $\varepsilon \in \mathcal{T}$ is a random perturbation map [8]. We define $T_j(x_j) = T_{\mathbb{E}_{\oplus g_j}(X_j), g_j(x_j)} \in \mathcal{T}$, and

$$\begin{aligned} M_{\oplus j}(\omega, x_j; \nu) &= \mathbb{E} \left[d^2(Z_j(X_j)(\nu), \omega) \mid X_j = x_j \right], \\ M_{\oplus j}^L(\omega, x_j; \nu) &= \mathbb{E} \left[w(x_j, h) d^2(Z_j(X_j)(\nu), \omega) \right], \\ \hat{M}_{\oplus j}^L(\omega, x_j; \nu) &= \frac{1}{n} \sum_{i=1}^n \hat{w}_i(x_j, h) d^2(Z_{i,j}(X_{i,j})(\nu), \omega), \end{aligned}$$

where $Z_{i,j}(X_{i,j})(\nu) = [\varepsilon_i \circ T_j(X_{i,j})](\nu) \in \mathcal{M}$.

By definition we have

$$\begin{aligned} T_j(x_j)(\nu) &= \arg \min_{\omega \in \mathcal{M}} M_{\oplus j}(\omega, x_j; \nu), \\ T_j^L(x_j)(\nu) &= \arg \min_{\omega \in \mathcal{M}} M_{\oplus j}^L(\omega, x_j; \nu), \\ \hat{T}_j^L(x_j)(\nu) &= \arg \min_{\omega \in \mathcal{M}} \hat{M}_{\oplus j}^L(\omega, x_j; \nu). \end{aligned}$$

We need the following assumptions:

- (A1) The kernel function K is a symmetric probability density function centered at zero. Furthermore, define $K_{kl} = \int_{\mathbb{R}} K^k(u) u^l du$, where $|K_{14}|$ and $|K_{26}|$ are both finite.
- (A2) For all $j = 1, \dots, p$, the marginal density f_j of X_j as well as the conditional densities $f_{|z_j}(x_j)$ of $X_j \mid Z_j(x_j)(\nu) = z_j$ and $f_{|x_j}(z_j)$ of $Z_j \mid X_j = x_j$ exist. The conditional densities $f_{|z_j}(x_j)$ are twice continuously differentiable for all $z_j \in \mathcal{M}$ and $\sup_{x_j, z_j} |f''_{|z_j}(x_j)| < \infty$. For any open set $U \subset \mathcal{M}$, $\int_U dF_{|x_j}(z_j)$ is continuous in $x_j \in \mathcal{X}_j$, where $F_{|x_j}(z_j)$ is the cumulative distribution function corresponding to $f_{|x_j}(z_j)$.
- (A3) For all $\nu \in \mathcal{M}$, and $x_j \in \mathcal{X}_j$, $j = 1, \dots, p$, objects $T_j(x_j)(\nu)$, $T_j^L(x_j)(\nu)$, and $\hat{T}_j^L(x_j)(\nu)$ exist and are unique, the latter almost surely. For all $\delta > 0$,

$$\begin{aligned} \inf_{d(\omega, T_j(x_j)(\nu)) < \delta} [M_{\oplus j}(\omega, x_j; \nu) - M_{\oplus j}(T_j(x_j)(\nu), x_j; \nu)] &> 0, \\ \liminf_{h \rightarrow 0} \inf_{d(\omega, T_j^L(x_j)(\nu)) < \delta} [M_{\oplus j}^L(\omega, x_j; \nu) - M_{\oplus j}^L(T_j^L(x_j)(\nu), x_j; \nu)] &> 0. \end{aligned}$$

Condition (A1) is standard kernel requirements typically assumed in local regression estimation. Condition (A2) is distributional assumptions on the predictors and responses for the convergence of Fréchet regression estimators [33]. Condition (A3) is a regularity condition commonly used to establish the consistency of M-estimators [38].

We need the following assumption on the geodesic optimal transport:

- (A4) (Small Error Assumption) For perturbation maps $\{\varepsilon_{i,n}\}_{i=1}^n$ with sample size n , there exists a sequence $\delta_n > 0$ with $\delta_n \rightarrow 0$ as $n \rightarrow \infty$, such that

$$\mathbb{E} [d(\varepsilon_{1,n}(\nu), \nu)] \leq \delta_n,$$

for all $\nu \in \mathcal{M}$.

- (A5) There exists a constant $C > 0$ such that

$$d(\Gamma(v_1, v_2, v_3), \Gamma(v'_1, v'_2, v'_3)) \leq C \{d(v_1, v'_1) + d(v_2, v'_2) + d(v_3, v'_3)\}$$

- (A6) The transport maps $T_j(\cdot) \in \mathcal{T}$ are perturbation maps, i.e., for all $\nu \in \mathcal{M}$,

$$\nu = \arg \min_{\omega \in \mathcal{M}} \mathbb{E} \{d^2(T_j(X_j)(\nu), \omega)\},$$

and

$$\inf_{d(\omega, \nu) > \delta} [\mathbb{E}d^2(T_j(X_j)(\nu), \omega) - \mathbb{E}d^2(T_j(X_j)(\nu), \nu)] > 0,$$

for any $\delta > 0$.

The small error assumption is standard in the theory of generalized nonparametric regression [18]. We extend this notion in condition (A4) to ensure that the partial transport residual $P_{\oplus j}$ does not deviate substantially from the transport $T_j(X_j)$. Condition (A5) holds for random objects in complete, non-positively curved metric spaces (Hadamard spaces) [46]. Examples include the space of univariate distributions with the Wasserstein metric and the space of symmetric positive definite (SPD) matrices under the log-Cholesky, log-Euclidean, Frobenius, or power-Frobenius metrics, all of which are Hadamard spaces. Condition (A6) is also satisfied in these settings. For distributional-valued response in Wasserstein space, let F_{X_j} , $F_{\oplus j}$, and F_ν be distribution functions, and $F_{X_j}^{-1}$, $F_{\oplus j}^{-1}$, and F_ν^{-1} their corresponding quantile functions of $g_j(x_j)$, $\mathbb{E}_{\oplus} g_j(X_j)$, and $\nu \in \mathcal{M}$. Then the transport map is represented as a quantile function $T_j(X_j)(\nu) = F_{X_j}^{-1} \circ F_{\oplus j} \circ F_\nu^{-1}$, and its Fréchet mean $F_{\oplus j}^{-1} \circ F_{\oplus j} \circ F_\nu^{-1} = F_\nu^{-1}$, so (A6) is satisfied. For SPD matrices with the log-Cholesky metric, the Cholesky decomposition yields a vector representation in Euclidean space, which directly implies that Condition (A6) holds. The same argument extends to other metrics on SPD matrices, including the Frobenius, and power-Frobenius metrics. The inequality in Condition (A6) serves as a regularity condition analogous to (A3), ensuring the consistency of M-estimators and the uniqueness of the population Fréchet mean.

A.2 Proof of Theorem 1

We need to show that for any $\nu \in \mathcal{M}$ and $x_j \in \mathcal{X}_j$, if the bandwidth $h \rightarrow 0$ and $nh \rightarrow \infty$, it holds that

$$d(T_j(x_j)(\nu), \hat{T}_j(x_j)(\nu)) = o_p(1),$$

where $\hat{T}_j(\nu)$ is the estimates for the proposed transport backfitting algorithm.

For fixed $\nu \in \mathcal{M}$ and $x_j \in \mathcal{X}_j$ for fixed j , we have

$$d\left(T_j(x_j)(\nu), \hat{T}_j(x_j)(\nu)\right) \leq d\left(T_j(x_j)(\nu), \hat{T}_j^L(x_j)(\nu)\right) + d\left(\hat{T}_j^L(x_j)(\nu), \hat{T}_j(x_j)(\nu)\right) \quad (\text{S.1})$$

By Lemma 1 and the proof Theorem 3 in the Supplement of [33], under conditions (A1)-(A3), we observe the bias term

$$d\left(T_j(x_j)(\nu), \hat{T}_j^L(x_j)(\nu)\right) = o(1), \quad (\text{S.2})$$

as the bandwidth $h \rightarrow 0$. Also, by Lemma 2 in the Supplement of [33], under conditions (A1) and (A3), we observe the stochastic term

$$d\left(\hat{T}_j^L(x_j)(\nu), \hat{T}_j(x_j)(\nu)\right) = o_p(1) \quad (\text{S.3})$$

as $h \rightarrow 0$ and $nh \rightarrow \infty$. Combining (S.2) and (S.3), we have the first term of (S.1)

$$d\left(T_j(x_j)(\nu), \hat{T}_j(x_j)(\nu)\right) = o_p(1) \quad (\text{S.4})$$

Thus, it is enough to show that the second term of (S.1)

$$d\left(\hat{T}_j^L(x_j)(\nu), \hat{T}_j(x_j)(\nu)\right) = o_p(1). \quad (\text{S.5})$$

By the transport backfitting algorithm we can represent,

$$\hat{T}_j(x_j)(\nu) = T_{\hat{\mathbb{E}}_{\oplus} \hat{g}_j(X_j), \hat{g}_j(x_j)}(\nu),$$

where

$$\begin{aligned} \hat{g}_j(x_j) &= \arg \min_{\omega \in \mathcal{M}} \frac{1}{n} \sum_{i=1}^n \hat{w}_i(x_j, h) d^2(P_{\oplus i, j}(\nu), \omega), \\ \hat{\mathbb{E}}_{\oplus} \hat{g}_j(X_j) &= \arg \min_{\omega \in \mathcal{M}} \frac{1}{n} \sum_{i=1}^n d^2(\hat{g}_j(X_{i, j}), \omega). \end{aligned}$$

By condition (A6) and the property of transport map, we have $\hat{T}_j^L(x_j)(\nu) = T_{\nu, \hat{T}_j^L(x_j)(\nu)}(\nu) = T_{\mathbb{E}_{\oplus} T_j(X_j)(\nu), \hat{T}_j^L(x_j)(\nu)}(\nu)$. The equation (S.5) is

$$\begin{aligned} d\left(\hat{T}_j^L(x_j)(\nu), \hat{T}_j(x_j)(\nu)\right) &= d\left(T_{\mathbb{E}_{\oplus} T_j(X_j)(\nu), \hat{T}_j^L(x_j)(\nu)}(\nu), T_{\mathbb{E}_{\oplus} \hat{g}_j(X_j), \hat{g}_j(x_j)}(\nu)\right) \\ &\leq C \left\{ d\left(\mathbb{E}_{\oplus} T_j(X_j)(\nu), \hat{\mathbb{E}}_{\oplus} \hat{g}_j(X_j)\right) + d\left(\hat{T}_j^L(x_j)(\nu), \hat{g}_j(x_j)\right) \right\}, \end{aligned}$$

for some constant $C > 0$, and the last inequality came from condition (A5).

Lemma 1 Under (A1), (A3), (A4), and (A5), if the bandwidth $h \rightarrow 0$ and $nh \rightarrow \infty$ as $n \rightarrow \infty$, it holds that

$$d\left(\hat{T}_j^L(x_j)(\nu), \hat{g}_j(x_j)\right) = o_P(1),$$

for any $x_j \in \mathcal{X}_j$, and $\nu \in \mathcal{M}$.

Lemma 2 Under (A1)-(A6), if the bandwidth $h \rightarrow 0$ and $nh \rightarrow \infty$ as $n \rightarrow \infty$, it holds that

$$d\left(\mathbb{E}_{\oplus} T_j(X_j)(\nu), \hat{\mathbb{E}}_{\oplus} \hat{g}_j(X_j)\right) = o_P(1),$$

for any $x_j \in \mathcal{X}_j$, and $\nu \in \mathcal{M}$.

Combining Lemma 1 and Lemma 2, we have $d\left(\hat{T}_j^L(x_j)(\nu), \hat{g}_j(x_j)\right) = o_p(1)$ and $d\left(\mathbb{E}_{\oplus} T_j(X_j)(\nu), \hat{\mathbb{E}}_{\oplus} \hat{g}_j(X_j)\right) = o_p(1)$, leading to the desired results in (S.5),

$$d\left(\hat{T}_j^L(x_j)(\nu), \hat{T}_j(x_j)(\nu)\right) = o_p(1).$$

Then, the equation (S.4) and (S.5) verifies our goal of (S.1),

$$d\left(T_j(x_j)(\nu), \hat{T}_j(x_j)(\nu)\right) = o_p(1).$$

A.3 Proof of Lemmas

A.3.1 Proof of Lemma 1

By Corollary 3.2.3 in [38], for the proof of the consistency of M-estimators $d\left(\hat{T}_j^L(x_j)(\nu), \hat{g}_j(x_j)\right) = o_p(1)$, it is sufficient to show that the uniform consistency of loss functions,

$$\sup_{\omega \in \mathcal{M}} \left| \frac{1}{n} \sum_{i=1}^n \hat{w}_i(x_j, h) d^2(Z_{i,j}(X_{i,j})(\nu), \omega) - \frac{1}{n} \sum_{i=1}^n \hat{w}_i(x_j, h) d^2(P_{\oplus i,j}(\nu), \omega) \right| = o_p(1).$$

Combining Theorem 1.3.6 and 1.5.4 of [38], we need to show that

- (1) (Pointwise consistency) $\frac{1}{n} \sum_{i=1}^n \hat{w}_i(x_j, h) d^2(Z_{i,j}(X_{i,j})(\nu), \omega) - \frac{1}{n} \sum_{i=1}^n \hat{w}_i(x_j, h) d^2(P_{\oplus i,j}(\nu), \omega) = o_p(1)$ for all $\omega \in \mathcal{M}$, and
- (2) (Asmptotically equicontinuous in probability) For all $\epsilon, \eta > 0$, there exists $\delta > 0$ such that

$$\limsup_n P \left(\sup_{d(\omega_1, \omega_2) < \delta} |A_n(\omega_1) - A_n(\omega_2)| > \epsilon \right) < \eta,$$

where $A_n(\omega) = \frac{1}{n} \sum_{i=1}^n \hat{w}_i(x_j, h) d^2(Z_{i,j}(X_{i,j})(\nu), \omega) - \frac{1}{n} \sum_{i=1}^n \hat{w}_i(x_j, h) d^2(P_{\oplus i,j}(\nu), \omega)$.

Begin with (1),

$$\begin{aligned}
& \left| \frac{1}{n} \sum_{i=1}^n \hat{w}_i(x_j, h) \left\{ d^2(Z_{i,j}(X_{i,j})(\nu), \omega) - d^2(P_{\oplus i,j}(\nu), \omega) \right\} \right| \\
&= \left| \frac{1}{n} \sum_{i=1}^n \hat{w}_i(x_j, h) \left\{ d^2([\varepsilon_{i,n} \circ T_j(X_{i,j})](\nu), \omega) \right. \right. \\
&\quad \left. \left. - d^2([T_{j+1}^{-1}(X_{i,j+1}) \circ \cdots \circ T_p^{-1}(X_{i,p}) \circ \varepsilon_{i,n} \circ T_p(X_{i,p}) \circ \cdots \circ T_{j+1}(X_{i,j+1}) \circ T_j(X_{i,j})](\nu), \omega) \right\} \right| \\
&\leq 2\text{diam}(\mathcal{M}) \\
&\times \frac{1}{n} \sum_{i=1}^n \hat{w}_i(x_j, h) d([\varepsilon_{i,n} \circ T_j(X_{i,j})](\nu), [T_{j+1}^{-1}(X_{i,j+1}) \circ \cdots \circ T_p^{-1}(X_{i,p}) \circ \varepsilon_{i,n} \circ T_p(X_{i,p}) \circ \cdots \circ T_j(X_{i,j})](\nu)),
\end{aligned}$$

where the last inequality is from $d^2(a, \omega) - d^2(b, \omega) \leq |d(a, \omega) - d(b, \omega)|(d(a, \omega) + d(b, \omega)) \leq 2\text{diam}(\mathcal{M})d(a, b)$, for any $a, b \in \mathcal{M}$, and fixed $\omega \in \mathcal{M}$.

Lemma 3 Under conditions (A4) and (A5), it holds that

$$\frac{1}{n} \sum_{i=1}^n d([T \circ \varepsilon_{i,n}](\xi), [\varepsilon_{i,n} \circ T](\xi)) = o_p(1),$$

for any $T \in \mathcal{T}$, and $\xi \in \mathcal{M}$.

By Lemma 3 with $T = T_{j+1}^{-1}(X_{i,j+1}) \circ \cdots \circ T_p^{-1}(X_{i,p}) \in \mathcal{T}$ and $\xi = [T_p(X_{i,p}) \circ \cdots \circ T_j(X_{i,j})](\nu) \in \mathcal{M}$, we observe that

$$\frac{1}{n} \sum_{i=1}^n d([\varepsilon_{i,n} \circ T_j(X_{i,j})](\nu), [T_{j+1}^{-1}(X_{i,j+1}) \circ \cdots \circ T_p^{-1}(X_{i,p}) \circ \varepsilon_{i,n} \circ T_p(X_{i,p}) \circ \cdots \circ T_j(X_{i,j})](\nu)) = o_p(1).$$

Also, by Lemma 2 in Supplement of [33], $\frac{1}{n} \sum_{i=1}^n \hat{w}_i(x_j, h) = O_p(1)$, with $\hat{w}_i(x, h) > 0$ for all x . Since \mathcal{M} is bounded, we have

$$\left| \frac{1}{n} \sum_{i=1}^n \hat{w}_i(x_j, h) \left\{ d^2(Z_{i,j}(X_{i,j})(\nu), \omega) - d^2(P_{\oplus i,j}(\nu), \omega) \right\} \right| = o_p(1),$$

which is the pointwise consistency in (1).

Moving on to (2),

$$\begin{aligned}
|A_n(\omega_1) - A_n(\omega_2)| &= \frac{1}{n} \sum_{i=1}^n \hat{w}_i(x_j, h) \left\{ d^2(Z_{i,j}(X_{i,j})(\nu), \omega_1) - d^2(Z_{i,j}(X_{i,j})(\nu), \omega_2) \right\} \\
&\quad + \frac{1}{n} \sum_{i=1}^n \hat{w}_i(x_j, h) \left\{ d^2(P_{\oplus i,j}(\nu), \omega_1) - d^2(P_{\oplus i,j}(\nu), \omega_2) \right\} \\
&\leq 4\text{diam}(\mathcal{M})d(\omega_1, \omega_2) \frac{1}{n} \sum_{i=1}^n |\hat{w}_i(x_j, h)|.
\end{aligned}$$

Then, $\frac{1}{n} \sum_{i=1}^n |\hat{w}_i(x_j, h)| = O_p(1)$ leads to $|A_n(\omega_1) - A_n(\omega_2)| = O_p(d(\omega_1, \omega_2))$, which verifies (2).

A.3.2 Proof of Lemma 2

We observe

$$d\left(\mathbb{E}_{\oplus} T_j(X_j)(\nu), \hat{\mathbb{E}}_{\oplus} \hat{g}_j(X_j)\right) \leq d\left(\mathbb{E}_{\oplus} T_j(X_j)(\nu), \hat{\mathbb{E}}_{\oplus} T_j(X_j)(\nu)\right) + d\left(\hat{\mathbb{E}}_{\oplus} T_j(X_j)(\nu), \hat{\mathbb{E}}_{\oplus} \hat{g}_j(X_j)\right).$$

By [12], under condition (A6), the consistency of sample Fréchet mean holds, i.e.,

$$d\left(\mathbb{E}_{\oplus}T_j(X_j)(\nu), \hat{\mathbb{E}}_{\oplus}T_j(X_j)(\nu)\right) = o_p(1). \quad (\text{S.6})$$

Following proof of Lemma 1, for the proof of $d\left(\hat{\mathbb{E}}_{\oplus}T_j(X_j)(\nu), \hat{\mathbb{E}}_{\oplus}\hat{g}_j(X_j)\right) = o_p(1)$, it is sufficient to show that

$$\sup_{\omega \in \mathcal{M}} \left| \frac{1}{n} \sum_{i=1}^n d^2(\hat{g}_j(X_{i,j}), \omega) - \frac{1}{n} \sum_{i=1}^n d^2(T_j(X_{i,j}), \omega) \right| = o_p(1).$$

We observe

$$\begin{aligned} \sup_{\omega \in \mathcal{M}} \left| \frac{1}{n} \sum_{i=1}^n d^2(\hat{g}_j(X_{i,j}), \omega) - \frac{1}{n} \sum_{i=1}^n d^2(T_j(X_{i,j}), \omega) \right| &\leq 2\text{diam}(\mathcal{M}) \frac{1}{n} \sum_{i=1}^n d(\hat{g}_j(X_{i,j}), T_j(X_{i,j})) \\ &\leq 2\text{diam}(\mathcal{M}) \frac{1}{n} \sum_{i=1}^n \left\{ d(\hat{g}_j(X_{i,j}), \hat{T}_j^L(X_{i,j})) + d(\hat{T}_j^L(X_{i,j}), T_j(X_{i,j})) \right\}. \end{aligned}$$

By Lemma 1, the first term $\frac{1}{n} \sum_{i=1}^n d(\hat{g}_j(X_{i,j}), \hat{T}_j^L(X_{i,j})) = o_p(1)$ and by equation (S.4), the second term $\frac{1}{n} \sum_{i=1}^n d(\hat{T}_j^L(X_{i,j}), T_j(X_{i,j})) = o_p(1)$. Thus, we have

$$d\left(\hat{\mathbb{E}}_{\oplus}T_j(X_j)(\nu), \hat{\mathbb{E}}_{\oplus}\hat{g}_j(X_j)\right) = o_p(1). \quad (\text{S.7})$$

Combining (S.6) and (S.7), we verify

$$d\left(\mathbb{E}_{\oplus}T_j(X_j)(\nu), \hat{\mathbb{E}}_{\oplus}\hat{g}_j(X_j)\right) = o_p(1).$$

A.3.3 Proof of Lemma 3

For fixed $T \in \mathcal{T}$, and $\xi \in \mathcal{M}$, we observe

$$\begin{aligned} d([T \circ \varepsilon_{i,n}](\xi), [\varepsilon_{i,n} \circ T](\xi)) &\leq d([T \circ \varepsilon_{i,n}](\xi), T(\xi)) + d(T(\xi), [\varepsilon_{i,n} \circ T](\xi)) \\ &\leq Cd(\varepsilon_{i,n}(\xi), \xi) + d(T(\xi), [\varepsilon_{i,n} \circ T](\xi)), \end{aligned}$$

for constant $C > 0$. The first inequality is from triangle inequality, and second inequality is from condition (A5).

Then,

$$\begin{aligned} \frac{1}{n} \sum_{i=1}^n d([T \circ \varepsilon_{i,n}](\xi), [\varepsilon_{i,n} \circ T](\xi)) &\leq C \frac{1}{n} \sum_{i=1}^n d(\varepsilon_{i,n}(\xi), \xi) + \frac{1}{n} \sum_{i=1}^n d(T(\xi), [\varepsilon_{i,n} \circ T](\xi)) \\ &\rightarrow C\mathbb{E}[d(\varepsilon_{1,n}(\xi), \xi)] + \mathbb{E}[d(\varepsilon_{1,n}(T(\xi)), T(\xi))] \quad \text{by WLLN.} \end{aligned}$$

By condition (A4), we have

$$\frac{1}{n} \sum_{i=1}^n d([T \circ \varepsilon_{i,n}](\xi), [\varepsilon_{i,n} \circ T](\xi)) = o_p(1),$$

which is the desired results.

B Further details on Brain connectivity for fMRI data analysis

Brain signal analysis at the subject level relies on time series of Blood Oxygen Level Dependent (BOLD) signals, into a set of regions of interest (ROI). The coherence between pairwise ROIs is usually measured by Pearson correlation coefficients of the fMRI time series, leading to $l \times l$ correlation matrix for l ROIs. Alzheimer's disease has been found to be associated with anomalies in the functional integration of ROIs [2, 32]. The list of $l = 11$ ROIs used in the analysis is provided in Table S.1. Preprocessing was conducted in MATLAB using the Statistical Parametric

Table S.1: Brain region of interest (ROI) used in the analysis along with its ROI label [1].

Region Full Name	ROI Label
Anterior medial prefrontal cortex	MPFC
Posterior cingulate cortex	PCC
Dorsal medial prefrontal cortex	dMFPC
Temporal parietal junction	TPJ
Lateral temporal cortex	LTC
Temporal pole	TempP
Ventral medial prefrontal cortex	vMFPC
Posterior inferior parietal lobule	pIPL
Retrosplenial cortex	Rsp
Parahippocampal cortex	PHC
Hippocampal formation	HF+

Mapping (SPM12, www.fil.ion.ucl.ac.uk/spm) and the rs-fMRI Data Analysis Toolkit V1.8 (REST1.8, <https://rfmri.org/REST>); further details are available in [44].

The BOLD signals for each subject were collected over 0 to 270 seconds with $K = 136$ measurements available at two-second interval. We have 136×11 signal matrix S , and s_{kl} is the (k, l) th element of the signal matrix S and an 11×11 connectivity matrix response Y was obtained using Pearson correlation, defined as

$$(Y)_{l_1, l_2} = \frac{\sum_{k=1}^K (s_{kl_1} - \bar{s}_{l_1})(s_{kl_2} - \bar{s}_{l_2})}{\sqrt{\sum_{k=1}^K (s_{kl_1} - \bar{s}_{l_1})^2} \sqrt{\sum_{k=1}^K (s_{kl_2} - \bar{s}_{l_2})^2}},$$

with $\bar{s}_l = \frac{1}{K} \sum_{k=1}^K s_{kl}$, $l_1, l_2 = 1, 2, \dots, 11$. For Alzheimer's disease (AD) studies, cerebrospinal fluid (CSF) amyloid-beta ($A\beta$) concentration is a widely used marker of amyloid pathology, with lower $A\beta$ levels typically indicating greater AD risk [31, 19]. Also, the CSF phosphorylated tau (p-Tau) concentration is another established biomarker, where elevated pTau levels are strongly associated with AD pathology [24], with higher p-Tau typically indicating greater AD risk.